Tunable optical absorption and interactions in graphene via oxygen plasma

Iman Santoso,[1,2,4,6] Ram Sevak Singh,[2] Pranjal Kumar Gogoi,[1,2,3] Teguh Citra Asmara,[1,2,3] Dacheng Wei,[2] Wei Chen,[2,4,5] Andrew T. S. Wee,[2,4] Vitor M. Pereira,[2,4,*] and Andrivo Rusydi[1,2,3,†]

[1]*NUSNNI-NanoCore, National University of Singapore, Singapore 117576, Singapore*

[2]*Department of Physics, National University of Singapore, Singapore 117542, Singapore*

[3]*Singapore Synchrotron Light Source, National University of Singapore, 5 Research Link, Singapore 117603, Singapore*

[4]*Graphene Research Centre, Faculty of Science, National University of Singapore, Singapore 117546, Singapore*

[5]*Department of Chemistry, National University of Singapore, Singapore 117543, Singapore*

[6]*Jurusan Fisika,FMIPA, Universitas Gadjah Mada, BLS 21 Yogyakarta 55281, Indonesia*

(Received 24 September 2012; published 26 February 2014)

We report significant changes of optical conductivity (σ_1) in single-layer graphene induced by mild oxygen plasma exposure and explore the interplay between carrier doping, disorder, and many-body interactions from their signatures in the absorption spectrum. The first distinctive effect is the reduction of the excitonic binding energy that can be extracted from the renormalized saddle point resonance at 4.64 eV. Secondly, σ_1 is nearly completely suppressed ($\sigma_1 \ll \sigma_0$) below an exposure-dependent threshold in the near-infrared range. The clear steplike suppression follows the Pauli blocking behavior expected for doped monolayer graphene. The nearly zero residual conductivity below $\omega \sim 2E_F$ can be interpreted as arising from the weakening of the electronic self-energy. Our data shows that mild oxygen exposure can be used to controllably dope graphene without introducing the strong physical and chemical changes that are common in other approaches to oxidized graphene, allowing a controllable manipulation of the optical properties of graphene.

DOI: 10.1103/PhysRevB.89.075134 PACS number(s): 78.67.Wj, 73.22.Pr

I. INTRODUCTION

In the absence of disorder, the optical conductivity of graphene—carbon atoms arranged in a two-dimensional hexagonal lattice—displays many remarkable optical properties, including a broadband universal optical conductivity ($\sigma_0 = \pi e^2/2h$) in the infrared-to-visible range.[1–4] In the visible-ultraviolet range, the interplay between electron-electron (e-e) and electron-hole (e-h) interactions yields unique excitonic effects that renormalize and redshift the bare band structure saddle point resonance by ∼0.6 eV. This is clearly seen in the real part of the optical conductivity (σ_1) of graphene[3–9] and is one of the clear instances where explicit consideration of many-body interactions is required for an accurate description of the electronic properties of graphene. Recently, controlled disorder, such as defects, impurities, vacancies, and adatoms, has been studied intensively and proposed as a means to tailor the transport and optical properties of graphene.[10–15] For example, the functionalization of graphene using K, Rb (Ref. 16), and NO_2 (Ref. 17) have shown the large doping effects indicated by strong suppression of the absorption below $2E_F$ (E_F is Fermi energy). Here, we explore the optical response of graphene to controlled disorder induced by oxygen plasma exposure.

Mild oxygen plasma exposure has been widely used to produce graphene oxide. This dry method has numerous advantages, namely: the oxidation can take place rapidly, and it does not strongly modify the transport properties of graphene. It is known that this method introduces structural defects and electronic disorder due to the attachment of oxygen to carbon atoms, and to the reduction in the overall sp^2 order.[18] The fact that the oxygen arrives to the sample surface by a process of diffusion makes remote oxygen plasma treatment a clean way to control the amount of disorder in graphene.[18] However, plasma exposure can have very different outcomes in the optical and transport properties of graphene, depending on the intensity of irradiation that directly translates into the degree of disorder and amorphization of the resulting carbon lattice. Increased carrier densities, semiconducting transport behavior, and photoluminescence are frequently seen.[18,19] However, the electronic structure and correlation effects in graphene with controlled disorder through the optical spectroscopy technique remain unexplored. Hence, it is of great interest to study directly the optical absorption spectrum of these systems, and analyze the interplay between carrier doping, disorder, and many-body interactions from their signatures in the optical absorption spectrum.

Here, we study the evolution of optical conductivity $\sigma_1(\omega)$ of monolayer graphene in the frequency range of 0.5–5.3 eV under mild (low power, ∼6W) exposure to oxygen plasma. Single-layer graphene (SLG) was prepared on the surface of a copper foil via a low-pressure chemical vapor deposition (CVD) process and then transferred to a SiO_2 (300 nm)/Si substrate. Exposure of SLG to the oxygen plasma is done in successive steps. After each 2-second (t_s) exposure step, Raman scattering and spectroscopic ellipsometry (SE) measurements are performed on the sample. The Raman traces are used to follow the level of disorder and amorphization in the system following each exposure step. The SE measurements are used to directly measure $\sigma_1(\omega)$ in the spectral range 0.5–5.3 eV. As t_s increases, two important effects emerge in the optical conductivity: the decrease of the resonant saddle-point peak intensity at 4.6 eV, concomitant with a significant reduction of the excitonic binding energy, and the dramatic suppression of σ_1 (close to zero) for photon energies below 1 eV.

II. SAMPLE PREPARATIONS AND EXPERIMENTAL METHODS

A low-pressure chemical vapor deposition (CVD) process was used to prepare SLG. A copper foil was placed in the

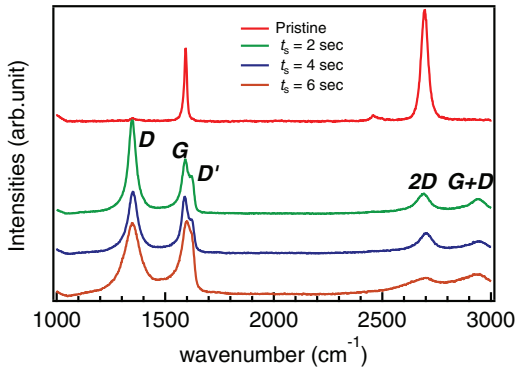

FIG. 1. (Color online) Raman spectra (excitation wavelength of 514 nm) for pristine single layer graphene (SLG) on SiO_2 (300 nm)/Si, and after consecutive intervals of oxygen plasma exposure: $t_s = 2$, 4, and 6 s.

center of a horizontal 2-inch quartz tube furnace and then was annealed at 1000 °C in 10-sccm (150 mTorr) H_2 for 30 min. After that, 30-sccm CH_4 was introduced into the furnace as the carbon source for SLG growth, while the H_2 was maintained at 10 sccm and the furnace temperature maintained at 1000 °C. The pressure was maintained at 350 mTorr in the growth. After 30 min, the CH_4 was turned off, and the furnace was quickly cooled down to room temperature in 10-sccm H_2. To transfer SLG to a SiO_2 (300 nm)/Si substrate, a PMMA film was spin-coated on the copper foil with SLG. After that, the copper foil was etched in $FeCl_3$ aqueous solution for 12 h, and then a PMMA film with SLG can be obtained on the solution surface. After cleaning the PMMA film in purified water several times, it was transferred to a SiO_2 (300 nm)/Si substrate and was heated at 180 °C for 2 min. To remove the PMMA, the substrate was placed in acetone vapor for 15 min and was annealed at 300 °C in 10-sccm H_2 for 30 min. The SLG sample was then exposed to the mild oxygen plasma for three consecutive durations of 2, 4, and 6 s using a radio-frequency (rf) plasma system. The rf power was maintained at 6W and chamber pressure at 50 mTorr. The pristine SLG and oxygen plasma exposed SLG were investigated using Raman and SE measurements. Raman spectra were recorded using a 514-nm laser excitation wavelength (Renishaw Raman measurement system). A low laser power of ∼2 mW is employed to minimize laser heating effects. All the measurements were performed at room temperature, in ambient, and on the same sample. To check the stability of the sample, we placed the sample in a dry box for one day after SE measurements. After that, we repeated the SE measurements, and the SE data showed no significant change, indicating that the sample is stable enough for measurements in an ambient environment.

Spectroscopic ellipsometry (SE) Refs. 20–22 measurements are performed on the graphene sample and substrate [SiO_2 (300 nm)/Si] using a SENTECH SE850 ellipsometer. This ellipsometer is equipped with three different light sources, i.e. deep UV (deuterium), UV/VIS source (Xe-lamp), and the NIR source [halogen lamp of the Fourier transform infrared (FT-IR) spectrometer], allowing us to measure from 0.5 to 6.3 eV. For our measurements, we used additional microfocus probes (∼100 micron spot diameter), which work well in the range from 0.5–5.3 eV. Spectroscopic ellipsometry allows the accurate measurement of ellipsometric parameters Ψ and Δ defined from the relation $\tan(\Psi)\exp(i\Delta) = \frac{r_p}{r_s}$, where r_p and r_s are the complex reflection amplitudes for the p and s light polarizations. Thus, Ψ represents the ratio between the amplitude of p- and s-polarized reflected light, while Δ represents the phase difference between p- and s-polarized reflected light.

III. RESULTS AND DISCUSSION

In Fig. 1, we show the Raman spectra for graphene on SiO_2 before (pristine) and after exposure to oxygen plasma for 2, 4, and 6 s. The high quality of our pristine graphene is confirmed by the very sharp Raman G peak at 1593 cm^{-1} with a full width at half maximum (FWHM) of 20 cm^{-1}, a two-dimensional (2D) peak at 2694 cm^{-1} with FWHM of 36 cm^{-1}, and no evidence of defect scattering (absent D peak). Furthermore, the 2D-to-G peak intensity ratio (I_{2D}/I_G) is around two, and the 2D peak possesses a symmetric single Lorentzian shape. This, together with the behavior of the σ_1 (see below) indicates that our system consists of monolayer graphene.[23] Upon exposure to oxygen plasma, the appearance of the D and D′ peaks at ∼1318 and 1615 cm^{-1}, respectively, indicates pronounced inter- and intravalley scattering.[19,23–25] After the first exposure, we observe a decrease in the ratio between the D and G peak intensities (I_D/I_G), which changes from 1.65 to 0.95 with growing t_s. The fact that the D and D′ peaks are intense and broad for $t_s > 2$s suggests relatively strong disorder. Furthermore, based on the three-stage model of structural disorder in graphitic materials,[26] our oxidized samples are likely in stage two. In this stage, the decrease of (I_D/I_G) is due to the decrease in the number of sp^2-ordered rings and is related to the in-plane crystalline grain size (L_a) through the empirical formula: $I_D/I_G = C'(\lambda)L_a^2$, where $C'(\lambda)$ denotes a constant at the particular excitation wavelength (λ) used in Raman measurements. Here, we use C′ (514 nm) = 0.55 nm^{-2}.[18,26]

Spectroscopy Ellipsometry data for Ψ and Δ are taken at multiple incident angles and at several spots on the sample. The data at different spots are identical in almost all cases which show sample homogeneity. The multiple incident angle data is required for global fitting of the data. SE measurement is generally preferable because it gives both the real and imaginary parts of the dielectric function directly, whereas other measurement techniques (such as direct reflectivity) require a Kramers-Kronig transformation. Moreover, in case of very thin films, the change in phase of the incident light waves upon reflection is much more pronounced than the change in amplitude of the light of different polarizations. These two facts make SE an ideal method for analyzing systems like the very thin monolayer of graphene on a substrate. In Fig. 2, we show the measured Ψ and Δ values of samples with and without graphene on substrate at 70° incident angle. The spectra show a pronounced contrast due to the presence of graphene which is only ∼3 Å thick.

We show the experimental Ψ and Δ of pristine graphene on the SiO_2 (300 nm)/Si substrate and after cumulative oxygen plasma exposure (t_s) in 2-s steps in Figs. 3(a) and 3(b). Due to oxygen plasma exposure, Ψ and Δ are slightly changed,

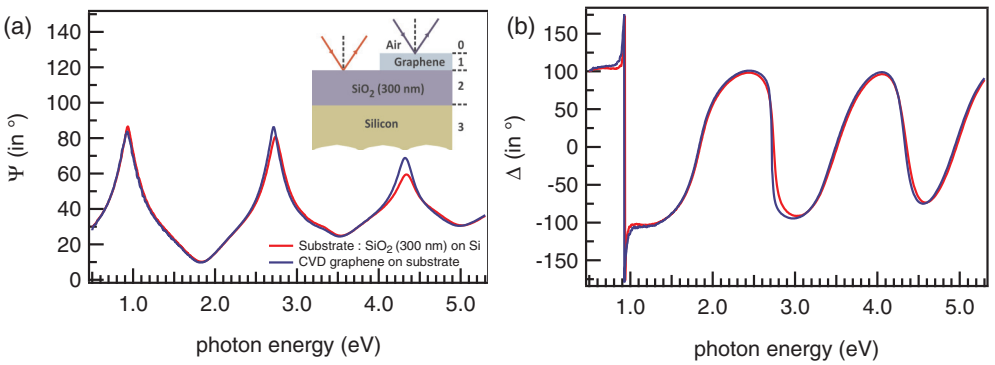

FIG. 2. (Color online) SE data of single layer chemical vapor deposition (CVD) graphene on SiO_2 (300 nm)/Si substrate. (a) Ψ and (b) Δ for substrate (CVD graphene) shown in red (blue). The inset in (a) shows the optical multilayer model used in extracting Ψ and Δ. Media 0, 1, 2, and 3 in the model denote air, a graphene layer with the thickness d_1 of 0.335 nm, a SiO_2 layer with the thickness d_2 of 300 nm, and silicon bulk, respectively.

especially in the energy range indicated in the inset of Figs. 3(a) and 3(b). These facts show that the optical constants (e.g. dielectric constant and hence optical conductivity) changed, and care should be taken when the fitting procedure is applied in these particular energy ranges. In contrast, within the error bars of the measurements, there is no significant change of the measured Ψ and Δ of the SiO_2 (300 nm)/Si substrate after cumulative oxygen plasma exposure [see Figs. 3(c) and 3(d) as well as the insets].

To extract the optical constants, the system is modeled with Fresnel coefficients for an optical multilayered film system [see inset of Fig. 2(a)]. The model is composed of a silicon bulk (label 3), a 300-nm SiO_2 layer (label 2), a 0.335-nm graphene layer (label 1), and the air (label 0). The Fresnel coefficients of reflected light for each interface of two adjacent layers are given by[20–22]

$$r_{01,p} = \frac{\sqrt{\varepsilon_1}\cos\theta_0 - \sqrt{\varepsilon_0}\cos\theta_1}{\sqrt{\varepsilon_1}\cos\theta_0 + \sqrt{\varepsilon_0}\cos\theta_1};$$
$$r_{01,s} = \frac{\sqrt{\varepsilon_0}\cos\theta_0 - \sqrt{\varepsilon_1}\cos\theta_1}{\sqrt{\varepsilon_0}\cos\theta_0 + \sqrt{\varepsilon_1}\cos\theta_1}, \quad (1)$$

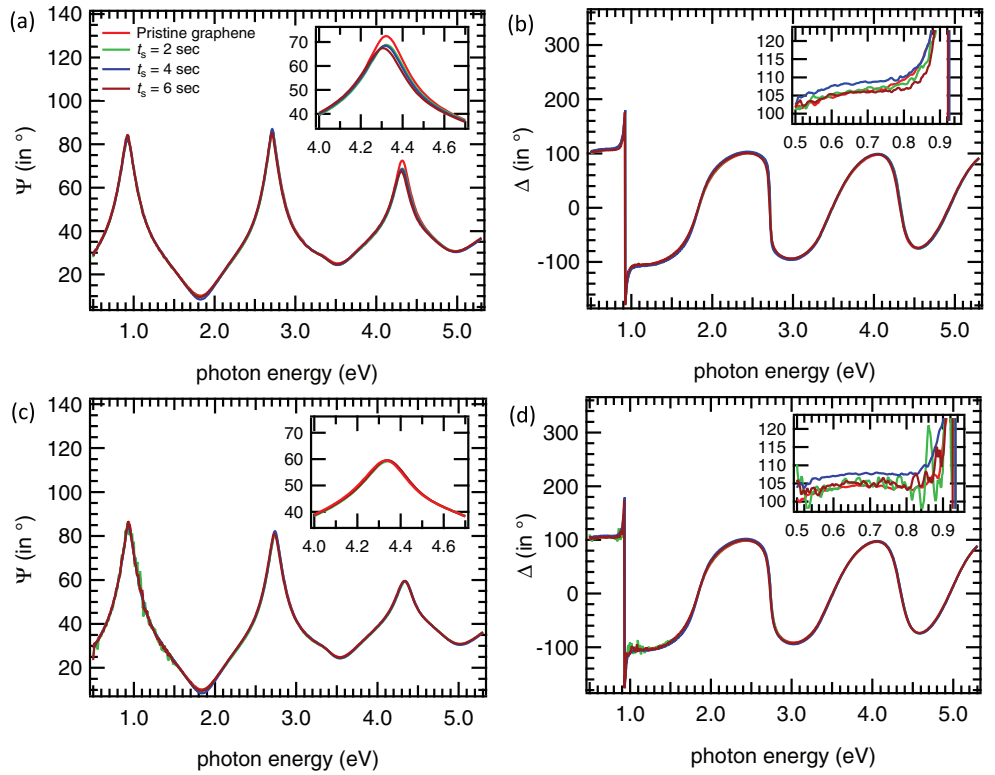

FIG. 3. (Color online) The experimental (a) Ψ and (b) Δ at an incident angle (θ_0) of 70° for pristine graphene on SiO_2 (300 nm)/Si substrate and after cumulative oxygen plasma exposure (t_s) in 2-s steps. The experimental (c) Ψ and (d) Δ of SiO_2 (300 nm)/Si substrate at an incident angle (θ_0) of 70°. The insets amplify Ψ and Δ at particular energy ranges.

where we have implicitly applied the Fresnel equation for the interface between medium 0 (air) and medium 1 (graphene layer) in deriving Eq. (1). The p and s denote the p and s polarization of light, respectively. The ε_0 and ε_1 represent the dielectric constant of medium 0 and medium 1. Here, θ_0 and θ_1 represent the incident angle and refracted angle at the interface between medium 0 and medium 1. These angles are related to each other by Snell's law. The Fresnel coefficients of reflected light for other interfaces (e.g. r_{12} and r_{23}) can be obtained by substituting the index 0 and 1 in Eq. (1) with the respective index under consideration. The total amplitude of the reflection of the system given in the inset of Fig. 2(a) is[20–22]

$$r_{0123,p(s)} = \frac{r_{01,p(s)} + r_{12,p(s)} \exp(-i2\beta_1) + [r_{01,p(s)} r_{12,p(s)} + \exp(-i2\beta_1)] r_{23,p(s)} \exp(-i2\beta_2)}{1 + r_{01,p(s)} r_{12,p(s)} \exp(-i2\beta_1) + [r_{12,p(s)} + r_{01,p(s)} \exp(-i2\beta_1)] r_{23,p(s)} \exp(-i2\beta_2)}, \tag{2}$$

where $p(s)$ denotes $p(s)$ polarized light; β_1 and β_2 represent the phase difference when light penetrates through the interface between medium 0 and 1, and between medium 2 and 3, respectively. Here, β_1 and β_2 are given by $\beta_1 = \frac{2\pi d_1}{\lambda}[\varepsilon_1 - \varepsilon_0 \sin^2\theta_0]^{1/2}$ and $\beta_2 = \frac{2\pi d_2}{\lambda}[\varepsilon_2 - \varepsilon_0 \sin^2\theta_0]^{1/2}$. Also, d_1 and d_2 are the thickness of the layer 1 and layer 2,

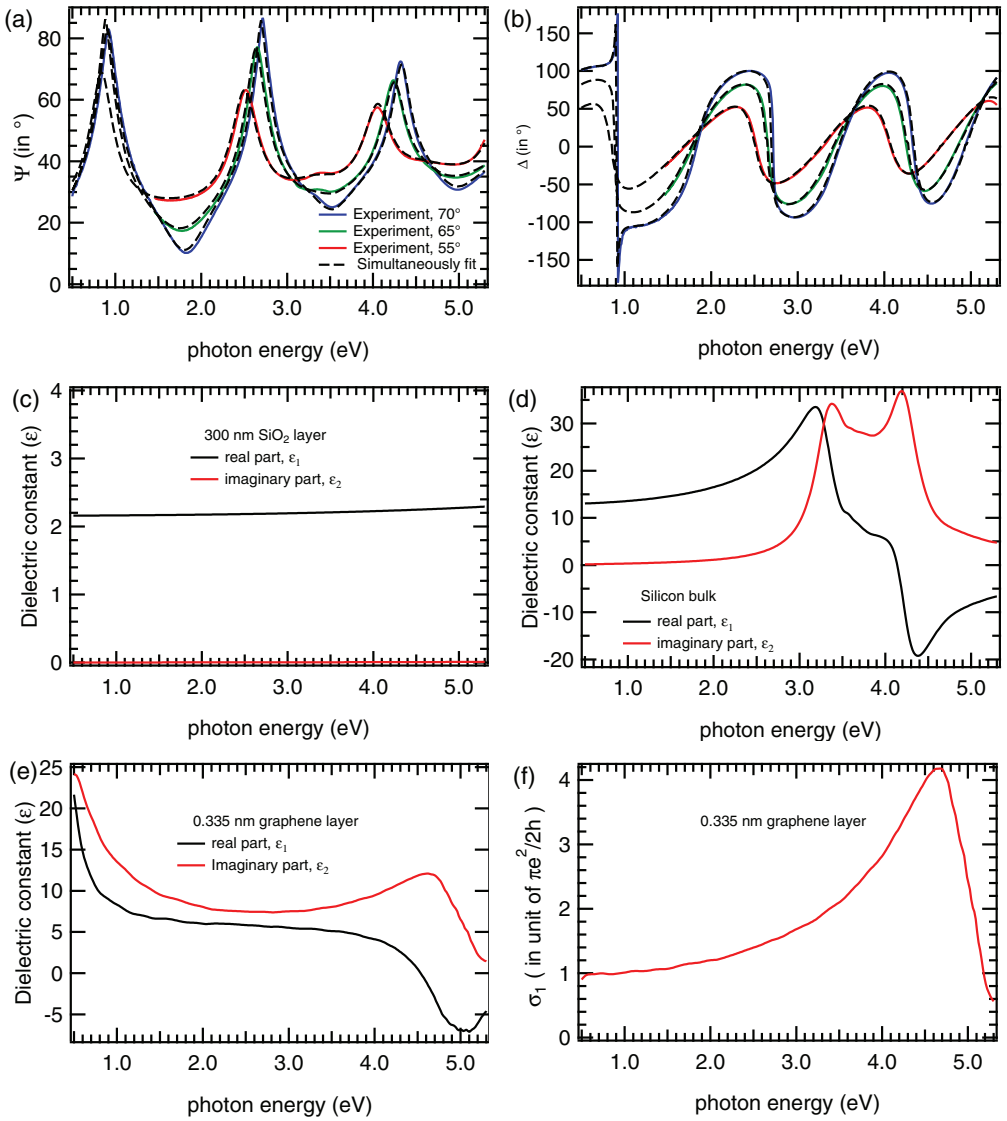

FIG. 4. (Color online) Detail of the analysis of SE data for pristine graphene on the SiO_2 (300 nm)/Si substrate. The experimental (a) Ψ and (b) Δ at different incident angles (θ_0) 70°, 65°, and 55° are shown in the solid blue, green, and red lines, respectively. The best match model extracted from the analysis is shown in dashed black lines. (c) Model dielectric constant used in the optical model for 300-nm SiO_2 layer. (d) Model dielectric constant used in the optical model for silicon bulk. (e) Model dielectric constant extracted from the optical model for the 0.335-nm graphene layer. (f) Corresponding optical conductivity of the graphene extracted from (e).

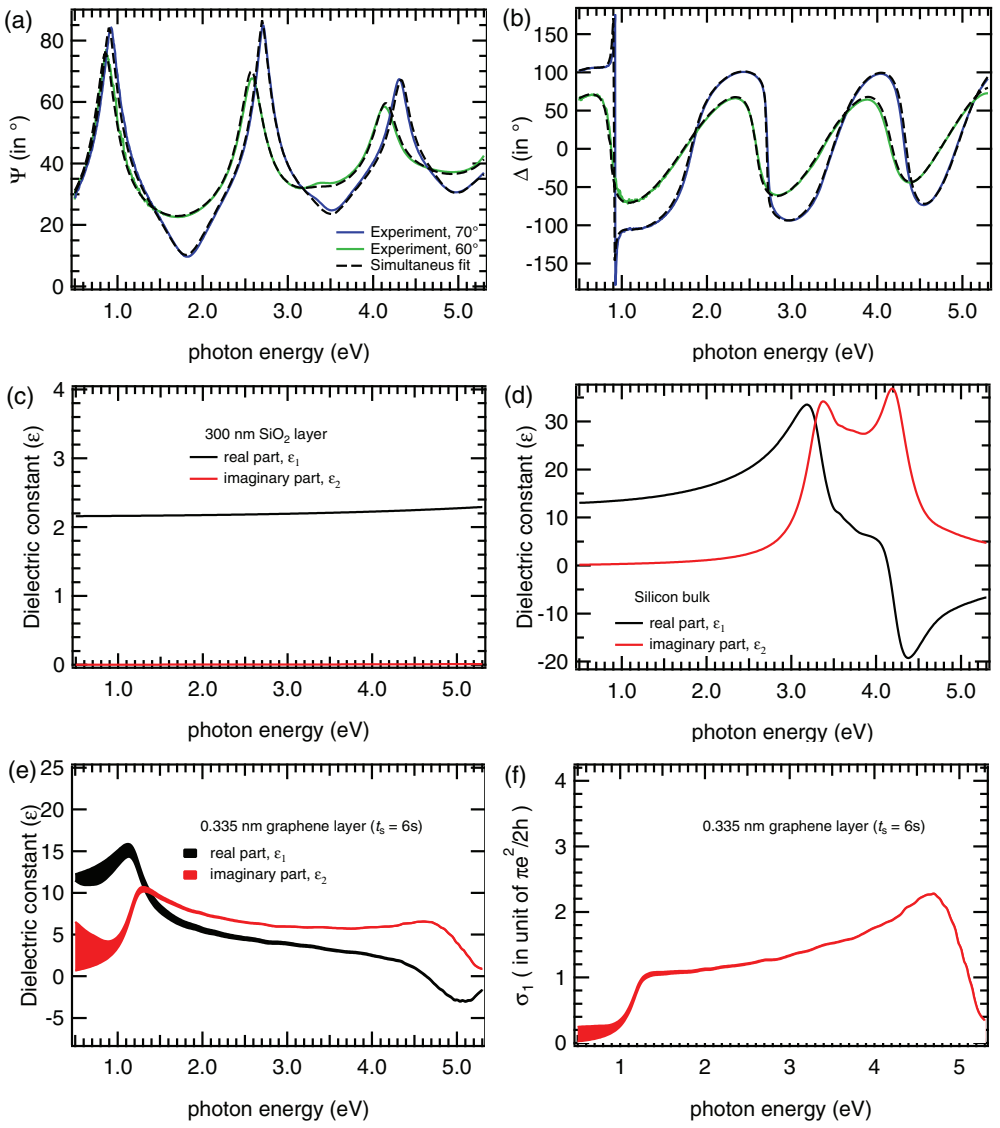

FIG. 5. (Color online) Detail of the analysis of SE data for graphene on the SiO_2 (300 nm)/Si substrate after 6s of oxygen plasma exposure time (t_s). The experimental (a) Ψ and (b) Δ at different incident angles (θ_0) 70° and 60° are shown in the solid blue and green lines, respectively. The best match model extracted from the analysis is shown in dashed black lines. (c) Model dielectric constant used in the optical model for the 300-nm SiO_2 layer. (d) Model dielectric constant used in the optical model for the silicon bulk. (e) Model dielectric constant ε_1 extracted from the optical model for 0.335-nm graphene layer. (f) Corresponding optical conductivity σ_1 of 0.335-nm graphene extracted from (e).

while λ denotes the wavelength of the light source used in this experiment.

The dielectric constants of the SiO_2 and silicon bulk are extracted from a fit of the experimental Ψ and Δ of the substrate with an optical model comprised of a 300-nm SiO_2 layer and silicon bulk [see the inset of Fig. 2(a) with red arrow]. In extracting these dielectric constants, we use many oscillators which can be described by Drude-Lorentz model:[21,22]

$$\varepsilon(\omega) = \varepsilon_\infty + \sum_k \frac{\omega_{p,k}^2}{\omega_{0,k}^2 - \omega^2 - i\gamma_k\omega}, \tag{3}$$

where ε_∞ denotes the high-frequency dielectric constant, which represents the contribution from all oscillators at very high frequencies compared to the frequency ranges under examination. The parameters $\omega_{p,k}, \omega_{o,k}$ and γ_k are the plasma frequency, the transverse frequency (eigenfrequency), and the line width (scattering rate), respectively, of the kth Lorentz oscillator. For the SiO_2 layer, we have used one additional oscillator at high energy (~9 eV) in order to capture the first absorption peak in SiO_2 (Ref. 27) and, hence, give the best match between the model and the experimental Ψ and Δ. Alternatively, one can use the Cauchy layer for describing the SiO_2 layer.[6] The obtained dielectric constants of the SiO_2 and silicon bulk used for extracting the dielectric constant of graphene based on the optical model are shown in the inset of Fig. 2(a) (with a blue arrow). We assume that the graphene film is flat and isotropic.[28–30] Having extracted the complex $\varepsilon(\omega) = \varepsilon_1(\omega) + i\varepsilon_2(\omega)$, $\sigma_1(\omega)$ follows immediately from

$$\sigma_1 = \frac{\omega\varepsilon_2}{4\pi}. \tag{4}$$

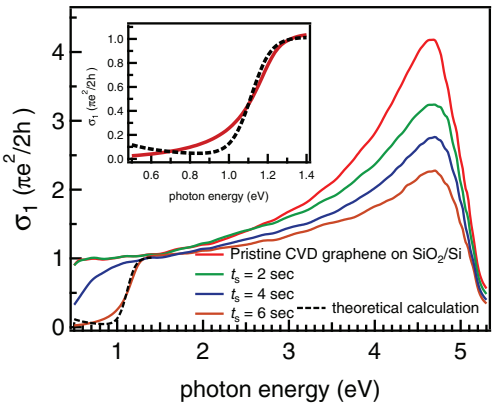

FIG. 6. (Color online) Corresponding real part of optical conductivity $\sigma_1(\omega)$ extracted from SE measurements. The dashed line below 1.4 eV is the best fit to the data for $t_s = 6$ s, as discussed in the text. The inset shows this fit in more detail.

Figures 4 and 5 plot the detailed analysis of SE data for pristine graphene on SiO_2 (300 nm)/Si substrate and after 6 s of oxygen plasma exposure time (t_s), respectively. The shaded area in ε_1 and σ_1 [Figs. 5(a) and 5(b)] indicates the range in which the model can still match the experimental Ψ and Δ (within the error bars).

In the next discussion, we concentrate on the evolution of σ_1 as function of t_s as shown in Fig. 6. In addition to the Raman characterization, the monolayer character of our sample is further corroborated by the constancy and magnitude of σ_1 at low frequencies, which rather accurately coincides with the universal value $\sigma_0 = \pi e^2/2h$ expected for a graphene monolayer.[31] The two main effects of oxygen exposure are: (1) a significant reduction (more than 50%) of the van Hove peak intensity at 4.64 eV in the ultraviolet (UV) range, accompanied by a large blueshift of the peak position; (2) σ_1 is gradually suppressed to zero in a steplike fashion as t_s increases in the near-infrared (NIR) range. We now discuss these two observations in more detail.

A prominent asymmetric peak in σ_1 at 4.64 eV can be attributed to excitonic renormalization of the independent particle optical transitions at the M point [i.e. van Hove singularity (VHS)] in the Brillouin zone of the graphene band structure. If one considers only direct band-to-band transitions using a local density approximation (LDA), the optical transition peak should occur at $\omega \sim 4.1$ eV. By accounting for e-e interactions within a GW (many-body) approach, the optical transition peak is predicted to lie at 5.2 eV, and further incorporating e-h interactions the peak is redshifted by ~600 meV from 5.2 to 4.6 eV.[4–8] This is precisely the position of the peak measured here for the pristine sample, as seen in Fig. 6.

In order to quantify the interplay between e-e and e-h interactions that manifests itself in the renormalization of the bare VHS peak in our controlled disorder graphene, we employ the Fano phenomenological approach since, as seen previously, the asymmetric peak measured here at 4.64 eV resembles a Fano profile. Following Fano's model, the asymmetric line shape in the optical spectra can be thought of as arising from the coupling of the continuum electronic states near the saddle point singularity (M point) to discrete sharp excitonic states.[32,33] The resultant σ_1 in the presence of this Fano resonance can be described by[7]

$$\frac{\sigma_1}{\sigma_{1,\mathrm{cont}}} = \frac{(q+\varepsilon)^2}{1+\varepsilon^2}, \tag{5}$$

where $\sigma_{1,\mathrm{cont}}(\omega)$ represents the continuum contribution to σ_1 arising from band-to-band transitions at the M point (possibly renormalized by e-e interactions[5]), $\varepsilon = \frac{2(\omega - E_{\mathrm{res}})}{\Gamma}$, Γ is a phenomenological width related to the lifetime of the exciton, and E_{res} denotes the resonance energy. The parameter q determines the line shape, while q^2 gives the ratio of the strength of the excitonic transition to the unperturbed band-to-band transition. For simplicity, to capture quantitatively the spectral features in the vicinity of the resonance, we model σ_{cont} with a constant background plus the logarithmic singularity in the joint density of states (JDOS) at the M point: $\sigma_{1,\mathrm{cont}}(\omega) = -A \log|1 - {}^{\omega}/_{E_0}| \otimes R_G(\omega) + C$, where A is a scaling factor, E_0 the unperturbed band-to-band transition energy, and $R_G(\omega)$ is a Gaussian of width $E_{Br} = 0.25$ eV that is convoluted with the bare divergence to account for the finite broadening.[7] The constant background (C) is intended to capture the universal optical conductivity (σ_0) of graphene at low frequencies.

Figure 7(a) shows the best fit of σ_1 for pristine single-layer graphene using the phenomenological Fano analysis with the parameters $q = -1.1$, $\Gamma = 0.93$ eV, $E_{\mathrm{res}} = 4.94$ eV, and $E_0 = 5.2$ eV. Despite the simplicity of the assumption used for σ_{cont}, the result of fitting Eq. (5) to the data in the energy range between 0.5 to 5.0 eV captures the overall behavior of the conductivity very well, including the universal σ_1 at lower energy and the main features of the renormalized van Hove peak. Figure 7(b) shows the separate contributions of $\sigma_{1,\mathrm{cont}}$ (upper panel) and the Fano resonance (lower panel) to the resulting σ_1, as a function of the oxygen exposure time. Figures 8(a)–8(c) show the dependence of Fano parameters q, Γ, E_{Res}, and E_0, respectively, on the amount of disorder. The symmetric peak at 5.25 eV in σ_{cont} coming from the unperturbed band-to-band transitions [see Fig. 7(b)] decreases significantly to 50% in intensity without any shift in energy, as quantified in Fig. 8(c). As for the contribution of the Fano resonance, it shows no significant change in shape as inferred from their q and Γ values, which barely change within the error bars [Figs. 2(a) and 2(b)]. However, a gradual blueshift as high as 100 meV is observed in the energy of the Fano resonance, as seen in Fig. 3(c), where we show the position of the Fano resonance and the peak in σ_{cont} that best fit each experimental curve for $\sigma_1(\omega)$. This variation of E_{Res} suggests a considerable reduction of the excitonic binding energy (by 100 meV for $t_s = 6$ s) upon oxygen exposure, whereas the persistence of the line shape indicates that, even though weakened upon oxygen exposure, the nature of the interaction itself has not changed. We consider now the dramatic suppression observed in σ_1 at frequencies below 1 eV. Oxygen plasma hole-dopes graphene and might, or might-not, introduce strong renormalization of the band structure, depending on the amount of disorder and how the oxidation affects the graphene lattice. Given that the overall profile of $\sigma_1(\omega)$ retains all the features of pristine graphene,

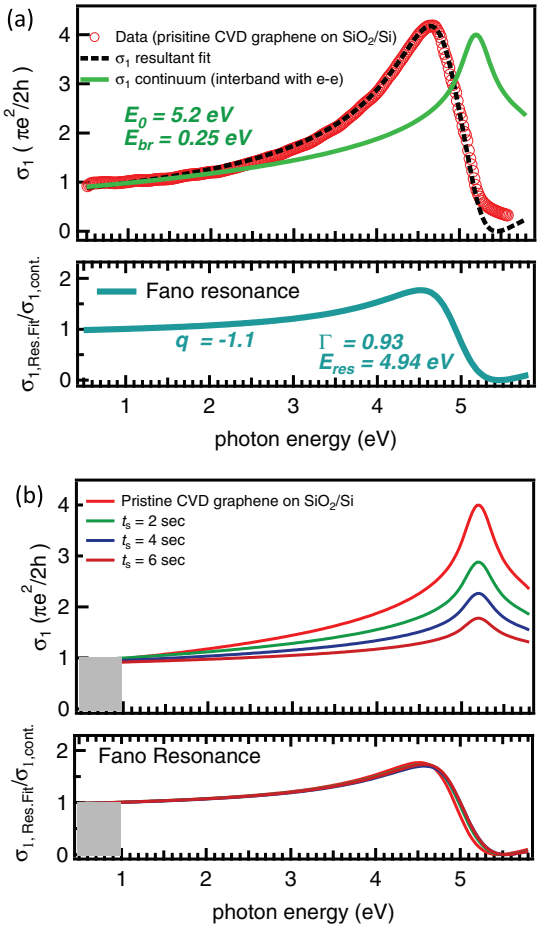

FIG. 7. (Color online) (a) Fit of the experimental conductivity using the phenomenological Fano line shape analysis discussed in the text for pristine single layer graphene on SiO_2 (300 nm)/Si. Upper panel: the optical conductivity σ_1 extracted from SE is shown as red circles, and the best fit to Eq. (1) by the dashed line; the unperturbed band-to-band component $\sigma_{\rm cont}$ is shown in green/solid. Lower panel: Isolated Fano contribution $\sigma_{\rm Res.Fit}/\sigma_{\rm cont}$. (b) Comparison of the two individual fitting components (unperturbed band-to-band transitions, upper panel, and Fano resonance profile, lower panel) as the oxygen plasma exposure time increased. The grey area denotes the low-energy region below $\sim 2E_F$ where σ_1 is Pauli-suppressed, which is not captured by the Fano approach.

we interpret the suppression of σ_1 at low frequencies as due to simple Pauli blocking, which excludes interband transitions for frequencies below $2E_F$ [see Figs. 9(b) and 4(c)].[2] For definiteness, and given that our lower experimental frequency limit is 0.5 eV, we explicitly compare the curve at the highest exposure time (that shows a clear suppression of absorption) with the expected frequency-dependent conductivity of doped SLG. Within a Kubo approach, it reads[34]

$$\frac{\sigma_1(\omega)}{\sigma_0} = \frac{8}{\pi}\left(\frac{2\gamma k_B T}{\omega^2+4\gamma^2}\right)\log\left[2\cosh\left(\frac{E_F}{2k_BT}\right)\right] + f\left(-\frac{\omega}{2}\right) - f\left(\frac{\omega}{2}\right), \quad (6)$$

where 2γ represents the half-width of the Drude peak and $f(E)$ is the usual Fermi-Dirac distribution function. The dashed

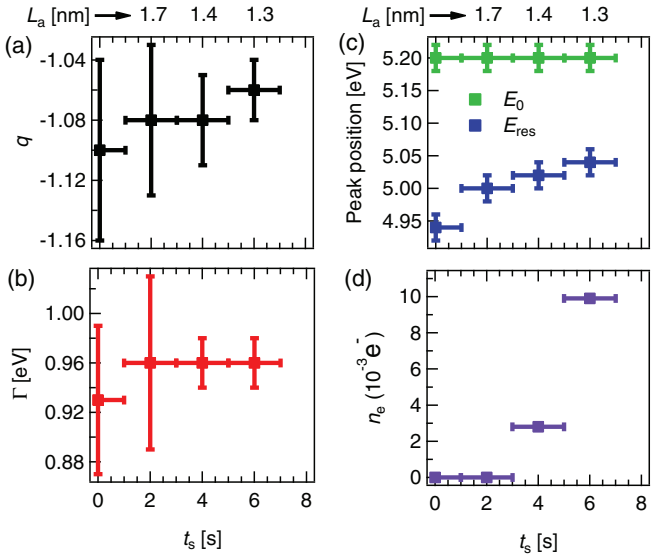

FIG. 8. (Color online) Fano parameters extracted from the fit of σ_1 as function of oxygen plasma exposure time t_s. The corresponding disorder parameter L_a (the in-plane crystalline grain size) derived from t_s is depicted on top of the graphs. (a) The Fano line shape parameter q. (b) The exciton lifetime within Fano's model. (c) The peak position of $\sigma_{\rm cont}$ (E_0), and Fano resonance energy ($E_{\rm res}$). (d) The number of charge carriers (n_e) extracted directly from the Pauli blocking seen in the experimental traces of $\sigma_1(\omega)$.

line below $\omega = 1.4$ eV in Fig. 6 shows the best fit of this expression to the experimental data at 300 K. From it, we obtain $E_F = 0.558 \pm 0.003$ eV and $\gamma = 0.021 \pm 0.004$ eV ($\approx$170 cm^{-1}). Despite the absence of data below 0.5 eV for direct confirmation, this value is in reasonable agreement with the Drude width expected for graphene grown by CVD on Cu under high electron doping (>100 cm^{-1}).[35] Assuming that the graphene dispersion remains linear after oxygen exposure, we can estimate the number of charge carriers (n_e) per unit cell as $n_e = A\frac{|E_F|^2}{\pi(\hbar v_F)^2}$, where A is the area of the graphene unit cell, and E_F can be extracted from the fit to the equation above. Figure 8(d) shows the dependence of n_e on oxygen exposure. Moreover, in graphene the integrated spectral weight (W) in the NIR is conserved, and density independent: $\int_0^{\omega_M}\sigma(\omega)d\omega \simeq \sigma_0\omega_M$, when the integration limit $\omega_M \gg 2E_F$. This integrated spectral weight is shown in Fig. 9(a) and allows us to check the consistency of the extracted E_F directly from the relative changes in optical spectral weight with different exposure times. The doping scenario is also consistent with the slight exposure-induced shift of the Raman G peak in our Raman data in Fig. 1.[18,36] The fact that the peak position changes only $\sim$40 meV [Fig. 8(c)] from $t_s = 2$ s to 6 s while n_e changes by an order of magnitude, [Fig. 8(d)] suggests the complex interplay between disorder and doping in the optical spectra.

What is striking in our optical data in this region is the very large suppression of σ_1 below $2E_F$ [Fig. 6, t_s = 6 s], when the optical response of doped graphene in the Pauli-blocked region is usually characterized by a residual conductivity $\sim$0.2–0.4 σ_0.[37] Such a residual conductivity can be justified theoretically on the basis of a finite electronic self-energy whose imaginary part is linear in ω.[38] The

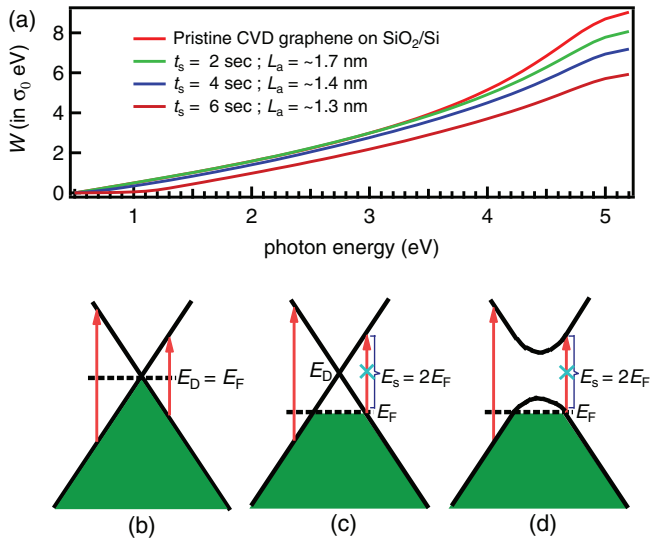

FIG. 9. (Color online) (a) The integrated optical spectral weight (W) up to the photon energies in the horizontal axis. (b) Allowed optical transitions (vertical red arrow) in pristine graphene. Here, E_d and E_F denotes the Dirac point and Fermi energy, respectively. (c) Likewise, for hole-doped graphene. Optical transitions below E_s are disallowed due to Pauli's exclusion principle. (d) In hole-doped and gapped graphene.

self-energy contributions can arise from the marginal Fermi liquid character of the electron-electron interactions in graphene, as well as optical phonons or disorder.[39,40] Our Raman data shows that the optical phonons are clearly affected by the oxygen exposure, and the Fano analysis of the optical data around the VHS reveals the clear suppression of the excitonic binding energy, thus hinting at reduced interactions with increased exposure times. Together these effects can lead to the suppression of the marginal Fermi liquid self-energy, thus explaining the nearly zero optical absorption below $2E_F$. Since our samples are disordered, it would also imply that the dominant mechanism for the residual optical conductivity in the Pauli-blocked region might indeed lie in interaction effects rather than disorder. Finally, we underline that our plasma exposure is much milder than the intensities employed in recent reports, which reveal pristine graphene transitioning from ambipolar metallic to insulating behavior upon treatment with oxygen plasma,[18,19] whereas our samples retain the overall graphene signature in the frequency-dependent optical conductivity.

IV. CONCLUSION

In summary, we reported ellipsometry and Raman spectroscopic measurements on monolayer graphene exposed to mild oxygen plasma. We see that it affects the magnitude of electronic interactions from the reduction of the excitonic binding energy in the UV range, and from the nearly zero residual optical conductivity in the Pauli-blocked NIR range, which, according to existing interpretations for that residual optical absorption, is consistent with the weakening of the electronic self-energy. Our data suggests, in addition, that low levels of oxygen plasma exposure can be used as a controllable means to tune the optical absorption in graphene, without disrupting the overall graphene optical response, contrary to what happens in other oxygenation or doping strategies. Finally, it remains an open question with regard to the IR spectral region below 0.5 eV, where important details might lie for the full picture of the effects of mild oxygenation, including details of the Drude region and spectral weight redistribution. The results reported here certainly warrant further investigation of this spectral region in the future.

ACKNOWLEDGMENTS

We are grateful to Antonio H. Castro Neto for very useful discussions. This work is supported by Singapore National Research Foundation under its Competitive Research Funding scheme of "Control of Exotic Quantum Phenomena at Strategic Interfaces and Surfaces for Novel Functionality by *in-situ* Synchrotron Radiation" (NRF-CRP 8-2011-06) and "Tailoring Oxide Electronics by Atomic Control" (NRF2008NRF-CRP002-024), and MOE-AcRF-Tier-2 (MOE2010-T2-2-121), NUS-YIA, and FRC. V.M.P. is supported by the NRF-CRP grant R-144-000-295-281.

*Corresponding author: vpereira@nus.edu.sg
†Corresponding author: phyandri@nus.edu.sg

[1] A. H. Castro Neto, F. Guinea, N. M. R. Peres, K. S. Novoselov, and A. K. Geim, Rev. Mod. Phys. **81**, 109 (2009).
[2] N. M. Peres, Rev. Mod. Phys. **82**, 2673 (2010).
[3] I. Santoso, P. K. Gogoi, H. B. Su, H. Huang, Y. Lu, D. Qi, W. Chen, M. A. Majidi, Y. P. Feng, A. T. S. Wee, K. P. Loh, T. Venkatesan, R. P. Saichu, A. Goos, A. Kotlov, M. Rüebhausen, and A. Rusydi, Phys. Rev. B **84**, 081403(R) (2011).
[4] P. K. Gogoi, I. Santoso, S. Saha, S. Wang, A. H. Castro Neto, K. P. Loh, T. Venkatesan, and A. Rusydi, Europhys. Lett. **99**, 67009 (2012).
[5] L. Yang, J. Deslippe, C. H. Park, M. L. Cohen, and S. G. Louie, Phys. Rev. Lett. **103**, 186802 (2009).
[6] V. G. Kravets, A. N. Grigorenko, R. R. Nair, P. Blake, S. Anissimova, K. S. Novoselov, and A. K. Geim, Phys. Rev. B **81**, 155413 (2010).
[7] K. F. Mak, J. Shan, and T. F. Heinz, Phys. Rev. Lett. **106**, 046401 (2011).
[8] D. H. Chae, T. Utikal, S. Weisenburger, H. Giessen, K. von Klitzing, M. Lippitz, and J. Smet, Nano Lett. **11**, 1379 (2011).
[9] V. N. Kotov, B. Uchoa, V. M. Pereira, F. Guinea, and A. H. Castro Neto, Rev. Mod. Phys. **84**, 1067 (2012).
[10] J. H. Chen, W. G. Cullen, C. Jang, M. S. Fuhrer, and E. D. Williams, Phys. Rev. Lett. **102**, 236805 (2009).
[11] J. H. Chen, C. Jang, S. Adam, M. S. Fuhrer, E. D. Williams, and M. Ishigami, Nat. Phys. **4**, 377 (2008).
[12] D. C. Elias, R. R. Nair, T. M. G. Mohiuddin, S. V. Morozov, P. Blake, M. P. Halsall, A. C. Ferrari, D. W. Boukhvalov, M. I. Katsnelson, A. K. Geim, and K. S. Novoselov, Science **323**, 610 (2009).
[13] T. O. Wehling, S. Yuan, A. I. Lichtenstein, A. K. Geim, and M. I. Katsnelson, Phys. Rev. Lett. **105**, 056802 (2010).
[14] S. Yuan, R. Roldán, H. De Raedt, and M. I. Katsnelson, Phys. Rev. B **84**, 195418 (2011).

[15] V. M. Pereira, F. Guinea, J. M. B. Lopes dos Santos, N. M. R. Peres, and A. H. Castro Neto, Phys. Rev. Lett. **96**, 036801 (2006).
[16] N. Jung, B. Kim, A. C. Crowther, N. Kim, C. Nuckolls, and L. Brus, ACS Nano **5**, 5708 (2011).
[17] A. C. Crowther, A. Ghassaei, N. Jung, and L. E. Brus, ACS Nano **6**, 1865 (2012).
[18] D. C. Kim, D. Y. Jeon, H. J. Chung, Y. S. Woo, J. K. Shin, and S. Seo, Nanotechnology **20**, 375703 (2009).
[19] A. Nourbakhsh, M. Cantoro, T. Vosch, G. Pourtois, F. Clamente, M. H. van der Veen, J. Hofkens, M. M. Heyns, S. D. Gendt, and B. F. Sels, Nanotechnology **21**, 435203 (2010).
[20] R. M. A. Azzam and N. M. Bashara, *Ellipsometry and Polarized Light* (North-Holland, Amsterdam, 1977).
[21] H. Fujiwara, *Spectroscopic Ellipsometry Principles and Applications* (John-Wiley and Sons, Tokyo, 2007).
[22] M. Born and E. Wolf, *Principles of Optics: Electromagnetic Theory of Propagation, Interference and Diffraction of Light*, 7th ed. (Cambridge University Press, Cambridge, 1999).
[23] A. C. Ferrari, J. C. Mayer, V. Scardaci, C. Casiraghi, M. Lazzeri, F. Mauri, S. Piscanec, D. Jiang, K. S. Novoselov, S. Roth, and A. K. Geim, Phys. Rev. Lett. **97**, 187401 (2006).
[24] L. G. Cancado, M. A. Pimenta, B. R. A. Neves, M. S. S. Dantas, and A. Jorio, Phys. Rev. Lett. **93**, 247401 (2004).
[25] M. A. Pimenta, G. Dresselhaus, M. S. Dresselhaus, L. G. Cancado, A. Jorio, and R. Saito, Phys. Chem. Chem. Phys. **9**, 1276 (2007).
[26] A. C. Ferrari and J. Robertson, Phys. Rev. B **61**, 14095 (2000).
[27] G. L. Tan, M. F. Lemon, D. J. Jones, and R. H. French, Phys. Rev. B **72**, 205117 (2005).
[28] F. J. Nelson, V. K. Kaminen, T. Zhang, E. S. Comfort, J. U. Lee, and A. C. Diebold, Appl. Phys. Lett. **97**, 253110 (2010).
[29] J. W. Weber, V. E. Calado, and M. C. M. van de Sanden, Appl. Phys. Lett. **97**, 091904 (2010).
[30] A. Boosalis, T. Hofmann, V. Darakchieva, R. Yakimova, and M. Schubert, Appl. Phys. Lett. **101**, 011914 (2012).
[31] R. R. Nair, P. Blake, A. N. Grigorenko, K. S. Novoselov, T. J. Booth, T. Stauber, N. M. R. Peres, and A. K. Geim, Science **320**, 1308 (2008).
[32] U. Fano, Phys. Rev. **124**, 1866 (1961).
[33] J. C. Phillips, in *Excitons. In The Optical Properties of Solids*, edited by J. Tauc (Academic Press, New York, 1966).
[34] V. P. Gusynin, S. G. Sharapov, and J. P. Carbotte, New J. Phys. **11**, 095013 (2009).
[35] J. Horng, C. F. Chen, B. Geng, C. Girit, Y. Zhang, Z. Hao, H. A. Bechtel, M. Martin, A. Zettl, M. F. Crommie, Y. R. Shen, and F. Wang, Phys. Rev. B **83**, 165113 (2011).
[36] J. Yan, Y. Zhang, P. Kim, and A. Pinczuk, Phys. Rev Lett. **98**, 166802 (2007).
[37] Z. Q. Li, E. A. Henriksen, Z. Jiang, Z. Hao, M. C. Martin, P. Kim, H. L. Stormer, and D. N. Basov, Nat. Phys. **4**, 532 (2008).
[38] A. G. Grushin, B. Valenzuela, and M. A. H. Vozmediano, Phys. Rev. B **80**, 155417 (2009).
[39] T. Stauber, N. M. R. Peres, and A. H. Castro Neto, Phys. Rev. B **78**, 085418 (2008).
[40] T. Ando, Y. Zheng, and H. Suzura, J. Phys. Soc. Jpn. **71**, 1318 (2002).